PROCEEDINGS OF SCIENCE

How Gluon Pseudo-PDF Matrix Elements Depend on Gauge Smearing

William Good[a,b,*] **and Huey-Wen Lin**[a]

[a] *Department of Physics and Astronomy, Michigan State University, East Lansing, MI 48824*

[b] *Department of Computational Math, Science, and Engineering, Michigan State University, East Lansing, MI 48824*

E-mail: goodwil9@msu.edu

We numerically study the effects of gauge smearing on the nucleon and meson gluon-PDF matrix elements, considering hypercubic smearing, stout smearing, and Wilson flow. The lattice calculations are carried out with $N_f = 2 + 1 + 1$ highly improved staggered quarks in ensembles generated by the MILC Collaboration. We use clover fermions for the valence action on one lattice spacing $a \approx 0.12$ fm and two pion masses $M_\pi \approx 310$ and 690 MeV. We probe the effects of gluon matrix elements with different smearing methods at various steps. We compute and compare the resulting nucleon and meson gluon PDFs using the pseudo-PDF method when using different smearing methods.

The 40th International Symposium on Lattice Field Theory (Lattice 2023)
July 31st - August 4th, 2023
Fermi National Accelerator Laboratory

*Speaker

PoS(LATTICE2023)330

1. Introduction

The gluon parton distribution functions (PDFs) of both the nucleon and the pion are informationally rich objects that are crucial to unraveling experimental data into meaningful results. The future U.S.- and China- based electron ion colliders are expected to expand our knowledge of the gluon PDF [1–4]; however, in the meantime, our understanding from global analysis is limited.

Lattice quantum chromodynamics (QCD) is a theoretical method for calculating nonperturbative QCD quantities, which has been used recently to calculate the gluon PDF. Ref. [5] reviews recent developments in the use of lattice QCD for PDFs while Ref. [6] gives an overview of the use of lattice QCD in hadron structure in general. In particular, it is difficult to obtain good signal-to-noise ratios for gluon observables from lattice QCD.

One method to improve signal in the matrix elements is to use gauge link smearing. A few common smearing methods are Hypercubic (HYP) smearing [7], Stout smearing [8], and Wilson flow [9]. An open question is how to compare these. Wilson flow is implemented as many small steps of Stout smearing and there has been some numerical exploration of their equivalency and how to relate them [10]. However, Stout and HYP smearing are not often directly compared systematically in the literature.

We study and compare the effects of different smearing methods in different amounts (steps) for the pseudo-PDF [11] matrix elements in the "light" and "strange" nucleons and mesons: N_l, N_s, π, $\eta_s = s\bar{s}$. We briefly consider the effects on the raw data and matrix element fits in the form of the ratio between the two-point and three-point correlators. We then explore the effects on the bare matrix elements and the Reduced Ioffe-time psuedo-distribution, defined later, before looking at the PDFs for a selection of the smearing types and amounts.

2. Lattice Setup, Correlators, and Matrix Elements

We calculate correlators on one ensemble with $N_\mathrm{f} = 2 + 1 + 1$ highly improved staggered quarks (HISQ) [12] generated by the MILC Collaboration [13], with lattice spacing $a \approx 0.12$ fm at "light" and "strange" pion masses $M_\pi \approx 310$ and 690 MeV. Each configuration initially has one step of hypercubic (HYP) smearing on the gauge links. Wilson-clover fermions are used in the valence sector, and the valence quark masses are tuned to reproduce the lightest light and strange sea pseudoscalar meson masses that were stated above.

We carry out our test by either applying further steps of HYP smearing or Stout smearing or by applying Wilson flow for some flow time. For HYP smearing, we use the parameters $\alpha_1 = 0.75$, $\alpha_2 = 0.6$, and $\alpha_3 = 0.3$ as defined in Ref. [7]. For Stout smearing, we use $\rho = 0.125$, and for Wilson flow we use n or $N_\mathrm{steps} = 100$. For the HYP and Stout smearing, we measure gluon loops on configurations with some number, X, of additional smearing steps are labeled "HYPX" or "STOUTX". Data from lattice with Wilson flow with flow time, T, are labeled "WILSONT". For all different smearing types, we use the same fit parameters for the matrix elements.

We measure the two-point (2pt) and three-point (3pt) correlators on the lattice defined as follows:

$$C_\mathrm{h}^{\mathrm{2pt}}(P_z; t_\mathrm{sep}) = \langle 0|\Gamma \int d^3y\, e^{-iyP_z} \chi(\vec{y}, t_\mathrm{sep}) \chi(\vec{0}, 0)|0\rangle, \tag{1}$$

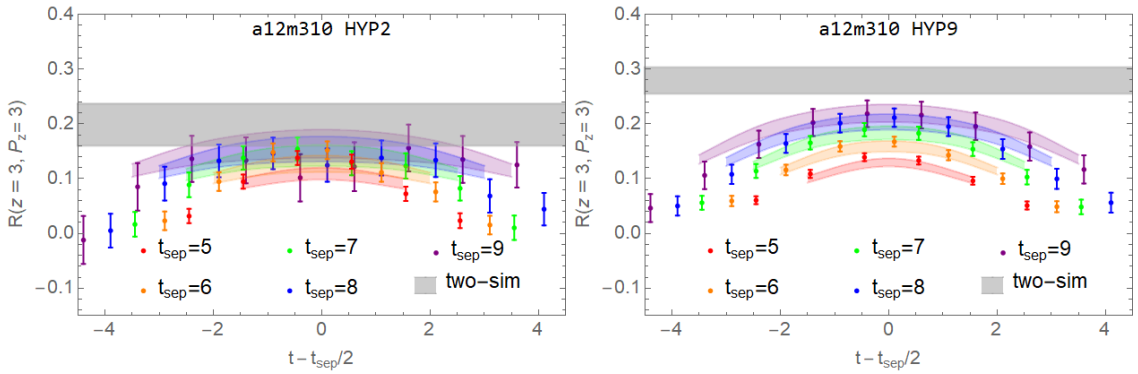

Figure 1: Example of two ratio plots for the two extreme samples of HYP smearing, HYP2 (left) and HYP9 (right), for the strange nucleon correlators at pion mass $M_\pi \approx 690$ MeV. The gray band on each plot gives the range for the ground-state matrix element extracted from the two-sim fits.

and

$$C_{\rm h}^{\rm 3pt}(z, P_z; t_{\rm sep}, t) = \langle 0|\Gamma \int d^3y\, e^{-iyP_z} \chi(\vec{y}, t_{\rm sep}) O_g(z, t) \chi(\vec{0}, 0)|0\rangle, \tag{2}$$

Here, χ is the interpolation operator for the given hadron. $\Gamma = \frac{1}{2}(1 + \gamma_4)$ is the projection operator. P_z is the hadron boost momentum in the z-direction. $t_{\rm sep}$ is the source-sink separation time, and t is the gluon-operator insertion time. $O_g(z, t)$ is the gluon operator from Ref. [14]:

$$O_g(z) \equiv \sum_{i \neq z,t} O(F^{ti}, F^{ti}; z) - \frac{1}{4} \sum_{i,j \neq z,t} O(F^{ij}, F^{ij}; z), \tag{3}$$

where the operator $O(F^{\mu\nu}, F^{\alpha\beta}; z) = F^{\mu}_{\nu}(z) U(z, 0) F^{\alpha}_{\beta}(0)$, and z is the Wilson link length. We used Gaussian momentum smearing [15] on the quark field and took $O(10^{5-6})$ measurements over ~1000 lattice configurations to allow for improved signal out to get a boost momenta of around 2 GeV.

To obtain the ground-state matrix element, we used a two-state fit on the 2pt correlators, and a two-sim fit on the 3pt correlators:

$$C_{\rm h}^{\rm 2pt}(P_z, t_{\rm sep}) = |A_{\rm h,0}|^2 e^{-E_{\rm h,0} t_{\rm sep}} + |A_{\rm h,1}|^2 e^{-E_{\rm h,1} t_{\rm sep}} + \ldots, \tag{4}$$

$$\begin{aligned} C_{\rm h}^{\rm 3pt}(z, P_z, t, t_{\rm sep}) = & \\ & |A_{\rm h,0}|^2 \langle 0|O_g|0\rangle e^{-E_{\rm h,0} t_{\rm sep}} + |A_{\rm h,0}||A_{\rm h,1}| \langle 0|O_g|1\rangle e^{-E_{\rm h,1}(t_{\rm sep} - t)} e^{-E_{\rm h,0} t} \\ & + |A_{\rm h,0}||A_{\rm h,1}| \langle 1|O_g|0\rangle e^{-E_{\rm h,0}(t_{\rm sep} - t)} e^{-E_{\rm h,1} t} + |A_{\rm h,1}|^2 \langle 1|O_g|1\rangle e^{-E_{\rm h,1} t_{\rm sep}} + \ldots \end{aligned} \tag{5}$$

where the $|A_{{\rm h},i}|^2$ and $E_{{\rm h},i}$ are the ground-state ($i = 0$) and first excited state ($i = 1$) amplitude and energy, respectively. We fit using three-point correlator data with $t_{\rm sep} \in [5, 9]$ and two-point correlator data with $t_{\rm sep} \in [2 - 11]$ for the nucleons and $[3, 15]$ for the mesons.

We plot the ratio of the three-point to the two-point correlators

$$R_{\rm h}(z, P_z, t_{\rm sep}, t) = \frac{C_{\rm h}^{\rm 3pt}(z, P_z, t, t_{\rm sep})}{C_{\rm h}^{\rm 2pt}(P_z, t_{\rm sep})}. \tag{6}$$

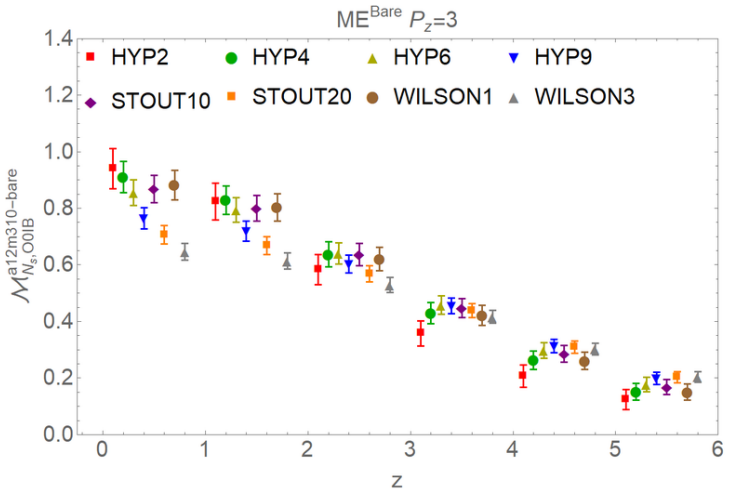

Figure 2: Comparison of the matrix elements across all sampled smearings for the strange nucleon correlators at pion mass $M_\pi \approx 690$ MeV at $P_z = 3$ in lattice units plotted against z in lattice units. The points are shifted for different smearings for clarity. The z value for the red HYP2 points represents the true z value for the bunch.

Ideally, as $t_{\text{sep}} \to \infty$, $R_N \to \langle 0|O_g|0\rangle$ as defined in Eq. 5. As a first look at the smearing effects, Fig. 1 compares smearings HYP2 and HYP9 for the strange nucleon at $z = 3$ and $P_z = 3$ in lattice units. The fitted matrix elements $\langle 0|O_g|0\rangle$ are shown as the gray band. As expected, HYP2 is noisier, while HYP9 is more clean. Both fits give a χ^2/dof within one standard deviation of 1, though HYP9 is slightly above and HYP2 is slightly below.

In Fig. 2, the fitted matrix elements for the strange nucleon at $P_z = 3$ are plotted versus z. The absolute values of the data cannot be directly compared due to different smearing amounts causing differences in the renormalization factors which are not removed at this stage. However, one can pick out some consistent relationships between the magnitudes that can be explored once the factors are removed. For example, STOUT10 and WILSON1 are both consistently between HYP4 and HYP6. Again, focusing just on HYP smearing, it is hard to determine what the signal-to-noise ratio is doing at small z, but at large z it is clear that the signal-to-noise ratio is increasing with more HYP smearing. Overall, similar patterns are seen in the matrix elements at other momenta and for other hadrons, but are not shown here for brevity.

3. RpITD Features

With our fitted ground-state matrix elements, we compute reduced Ioffe-time pseudo-distribution (RpITD) [11, 16–18]

$$\mathscr{M}(\nu, z^2) = \frac{\mathcal{M}(zP_z, z^2)/\mathcal{M}(0 \cdot P_z, 0)}{\mathcal{M}(z \cdot 0, z^2)/\mathcal{M}(0 \cdot 0, 0)}, \tag{7}$$

where Ioffe time $\nu = zP_z$, and $\mathcal{M}(\nu, z^2)$ are the matrix elements at boost momentum P_z and gluon operators with Wilson displacement z. By construction, the RpITD cancels renormalization and kinematic factors, removes the ultraviolet divergences are and reduces the lattice systematics. RpITDs act as input into the pseudo-PDF framework to obtain PDFs [11].

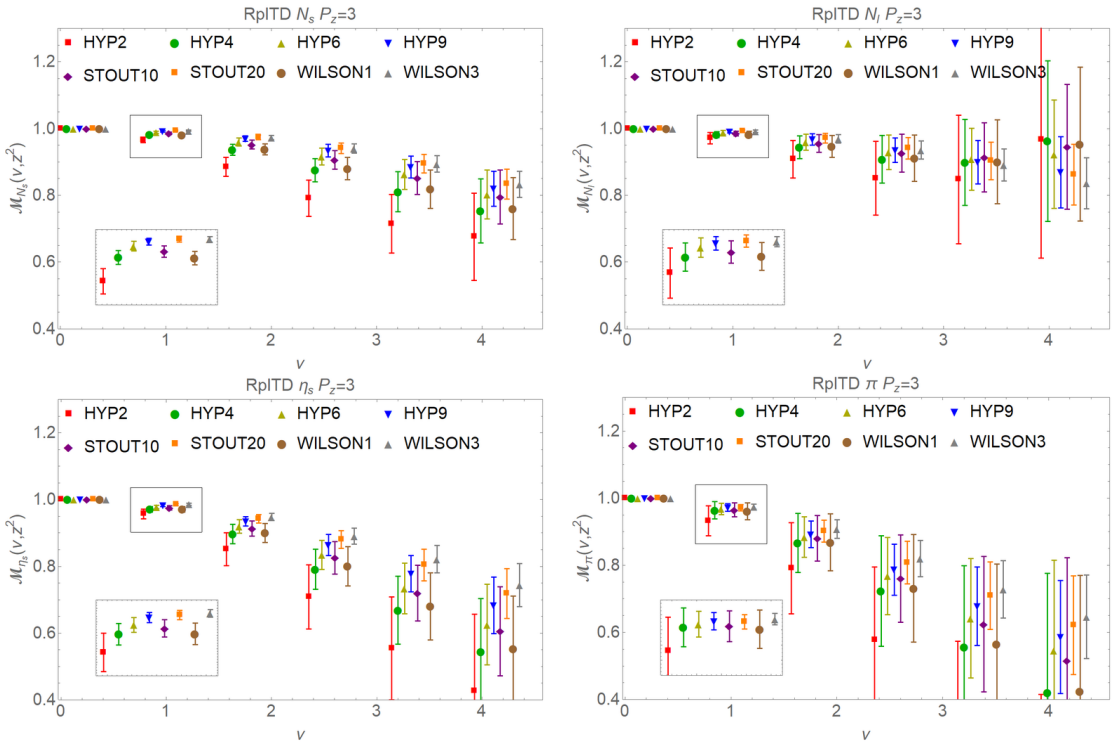

Figure 3: RpITDs for both strange and light nucleon and mesons, $M_\pi \approx 310$ and 690 MeV, across all sampled smearings. From top to bottom, left to right, the figures are strange nucleon, light nucleon, π, and η_s. The points are shifted for different smearings for clarity. The ν value for the red HYP2 points represents the true *nu* value for the bunch. The inset plots give a closer view of the points near $\nu = 1$. The points at $\nu = 0$ are identically 1.

The cancellation of renormalization factors allows us to directly compare RpITD values for different amounts of smearing. In Fig. 3, we present the RpITDs at $P_z = 3$ for all of the hadrons that we have considered. First, we observe the same patterns in relative magnitude between the STOUT10, WILSON1 and HYP4, HYP6 that was mentioned before in all hadrons. In many cases, the difference between magnitudes is not statistically significant, but the pattern in the mean values is universal, allowing one to make a rough comparison. Interestingly, looking at the nucleon in the top two plots, we see some slight tension between some of the largest and smallest smearing amounts in the low z data. Otherwise, the data mostly agree, and the increased smearing improves the signal-to-noise ratio. Another point of interest, there are competing trends in the nucleon at high z. Just looking at HYP2, as the pion mass decreases, the RpITD tends to increase unphysically. Increasing the smearing draws the data back down. In the bottom two plots for the pion and η_s, there is tension at all z between the largest and smallest smearing amounts. The trends here are opposite from the nucleons. Again, looking just at HYP2, decreasing the pion mass causes the RpITD to fall off much faster as z increases. The smearing then draws the data back up. Overall, it seems that the middle range of HYP smearing and lower Stout and Wilson data seem to all agree, and one may want to choose these amounts of smearing to have comparible results. We will explore this further by plotting some selected PDFs.

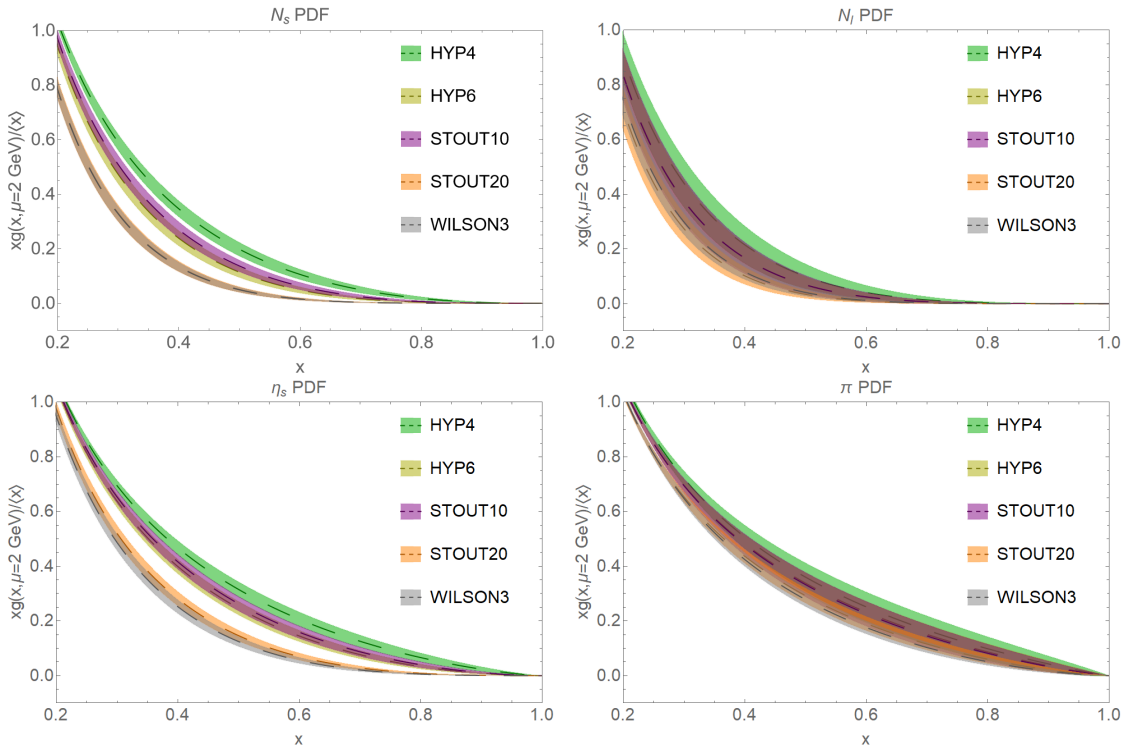

Figure 4: PDFs for both strange and light nucleon (top row) and mesons (bottom row), $M_\pi \approx 690$ (left column) and 310 MeV (right column), across some selected smearings. From top to bottom, left to right, the figures are strange nucleon, light nucleon, π, and η_s. The selected smearings are HYP5 (green), HYP7 (yellow), STOUT10 (purple), STOUT20 (Orange), WILSON3 (grey).

4. Preliminary Gluon PDF Comparison

We can extract the gluon PDF for a selection of smearings using the pseudo-PDF matching condition [14]

$$\mathscr{M}(\nu, z^2) = \int_0^1 dx \frac{xg(x,\mu^2)}{\langle x \rangle_g} R_{gg}(x\nu, z^2\mu^2), \tag{8}$$

where μ is the renormalization scale in the $\overline{\text{MS}}$ scheme and $\langle x \rangle_g = \int_0^1 dx\, xg(x,\mu^2)$ is the gluon momentum fraction. R_{gg} is the gluon-in-gluon matching kernel described in Ref. [14], which is used in several other studies on the gluon PDF from lattice QCD [19–22]. We ignore the quark contributions to the PDF and focus only focus on the normalized $xg(x,\mu^2)/\langle x \rangle_g$ for this study.

We obtain $xg(x,\mu^2)/\langle x \rangle_g$ by fitting the RpITD through the condition in Eq. 8 using a fit form commonly used in global analyses:

$$f_g(x,\mu) = \frac{xg(x,\mu)}{\langle x \rangle_g(\mu)} = \frac{x^A(1-x)^C}{B(A+1,C+1)}, \tag{9}$$

for $x \in [0,1]$ and zero elsewhere. The beta function $B(A+1,C+1) = \int_0^1 dx\, x^A(1-x)^C$ is used to normalize PDF properly.

We plot preliminary results of $xg(x,\mu^2)/\langle x\rangle_g$ for the different hadrons for our selection of smearings in Fig. 4. In all plots, we observe trends in the mean values that we expected from the RpITDs, such as STOUT10 being between HYP4 and HYP6. As expected, the larger error bars in the light hadrons wash out most differences between the different smearing types and amounts. Interestingly, there is even more tension than one would expect from the RpITDs in the strange PDFs. STOUT20 and WILSON3 are several standard deviations away from the other smearings in the mid-x range; however, it should be noted that the χ^2/dof is consistently larger for the strange hadrons, so a better fit form may need to be considered for these.

The same HYP4 results for the nucleon and meson are compared to PDFs from global analysis in Refs. [23] and [20].

5. Outlook and Conclusion

This study on the effects of smearing on several different gluon PDFs gives provides some key pieces of information for the a12m310 ensemble. We can draw some expected conclusions from a few examples of the ratio plots and fitted matrix elements. Mainly, we typically get better signal-to-noise ratio, at least in the mid- to high-z regions, without compromising χ^2/dof. The matrix elements suggest some comparison between the different smearing types, but only when we look at the RpITD can we confirm our suspicions. The RpITD shows that 10 steps of Stout smearing or Wilson flow for a flow time of 1 compare to somewhere between 4 and 6 steps of HYP smearing, for this ensemble and choice of parameters. Additionally, for the heavier pion mass hadrons, the RpITD suggests that the largest smearing amounts may be incompatible with the smaller- and middle-range data. Our PDF fits suggest that this is true even more than one would expect from the RpITD. The lighter PDFs all agree, while there is significant tension in the "strange" hadrons. Different fit forms may need to be considered for the strange hadrons.

All of these conclusions can only be made for our ensemble choice. Perhaps a finer lattice spacing would remove some of the inconsistencies. Some groups that use Wilson flow extrapolate to zero flow time. It would be interesting to explore this compared to the finite flow time and other smearing types. We use only one choice of smearing parameters for the HYP and Stout smearing. One could explore the effects of changing the parameters here. Further, one could additionally fill in more gaps in the smearing steps to get a better picture of the effects. As always, more two-point correlator data could give a cleaner signal, allowing us to make stronger claims about the relationships between the results.

This study is a good start and shows that smearing produces expected results, but not all of the effects should be ignored for cleaner signals. There is much further exploration that could be done numerically and mathematically.

Acknowledgments

We thank MILC Collaboration for sharing the lattices used to perform this study. The LQCD calculations were performed using the Chroma software suite [24]. We thank Alison Chevis for her help with grammatical and spelling edits in this draft. This research used resources of the National Energy Research Scientific Computing Center, a DOE Office of Science User Facility

supported by the Office of Science of the U.S. Department of Energy under Contract No. DE-AC02-05CH11231 through ERCAP, and facilities of the USQCD Collaboration, which are funded by the Office of Science of the U.S. Department of Energy. The work of WG is supported by partially by MSU University Distinguished Fellowship. The work of HL is partially supported by the US National Science Foundation under grant PHY 1653405 "CAREER: Constraining Parton Distribution Functions for New-Physics Searches", grant PHY 2209424, and by the Research Corporation for Science Advancement through the Cottrell Scholar Award.

References

[1] J. Arrington et al. Revealing the structure of light pseudoscalar mesons at the electron–ion collider. *J. Phys. G*, 48(7):075106, 2021. doi: 10.1088/1361-6471/abf5c3.

[2] Arlene C. Aguilar et al. Pion and Kaon Structure at the Electron-Ion Collider. *Eur. Phys. J. A*, 55(10):190, 2019. doi: 10.1140/epja/i2019-12885-0.

[3] R. Abdul Khalek et al. Science Requirements and Detector Concepts for the Electron-Ion Collider: EIC Yellow Report. *Nucl. Phys. A*, 1026:122447, 2022. doi: 10.1016/j.nuclphysa.2022.122447.

[4] Daniele P. Anderle et al. Electron-ion collider in China. *Front. Phys. (Beijing)*, 16(6):64701, 2021. doi: 10.1007/s11467-021-1062-0.

[5] Krzysztof Cichy. Progress in x-dependent partonic distributions from lattice qcd, 2021.

[6] Huey-Wen Lin. Overview of Lattice Results for Hadron Structure. *Few Body Syst.*, 64, 2023. doi: 10.1007/s00601-023-01842-9.

[7] Anna Hasenfratz and Francesco Knechtli. Flavor symmetry and the static potential with hypercubic blocking. *Phys. Rev. D*, 64:034504, 2001. doi: 10.1103/PhysRevD.64.034504.

[8] Colin Morningstar and Mike Peardon. Analytic smearing of SU(3) link variables in lattice qcd. *Phys. Rev. D*, 69:054501, Mar 2004. doi: 10.1103/PhysRevD.69.054501.

[9] Martin Lüscher. Properties and uses of the wilson flow in lattice qcd. *JHEP*, 71:054501, Aug 2010. doi: 10.1007/JHEP08(2010)071.

[10] Masato Nagatsuka, Keita Sakai, and Shoichi Sasaki. On the equivalence between the wilson flow and stout-link smearing, 2023.

[11] A. V. Radyushkin. Quasi-parton distribution functions, momentum distributions, and pseudo-parton distribution functions. *Phys. Rev. D*, 96(3):034025, 2017. doi: 10.1103/PhysRevD.96.034025.

[12] E. Follana, Q. Mason, C. Davies, K. Hornbostel, G. P. Lepage, J. Shigemitsu, H. Trottier, and K. Wong. Highly improved staggered quarks on the lattice, with applications to charm physics. *Phys. Rev. D*, 75:054502, 2007. doi: 10.1103/PhysRevD.75.054502.

[13] A. Bazavov et al. Lattice QCD Ensembles with Four Flavors of Highly Improved Staggered Quarks. *Phys. Rev. D*, 87(5):054505, 2013. doi: 10.1103/PhysRevD.87.054505.

[14] Ian Balitsky, Wayne Morris, and Anatoly Radyushkin. Gluon Pseudo-Distributions at Short Distances: Forward Case. *Phys. Lett. B*, 808:135621, 2020. doi: 10.1016/j.physletb.2020.135621.

[15] Gunnar S. Bali, Bernhard Lang, Bernhard U. Musch, and Andreas Schäfer. Novel quark smearing for hadrons with high momenta in lattice QCD. *Phys. Rev. D*, 93(9):094515, 2016. doi: 10.1103/PhysRevD.93.094515.

[16] Kostas Orginos, Anatoly Radyushkin, Joseph Karpie, and Savvas Zafeiropoulos. Lattice QCD exploration of parton pseudo-distribution functions. *Phys. Rev. D*, 96(9):094503, 2017. doi: 10.1103/PhysRevD.96.094503.

[17] Jian-Hui Zhang, Xiangdong Ji, Andreas Schäfer, Wei Wang, and Shuai Zhao. Accessing Gluon Parton Distributions in Large Momentum Effective Theory. *Phys. Rev. Lett.*, 122(14):142001, 2019. doi: 10.1103/PhysRevLett.122.142001.

[18] Zheng-Yang Li, Yan-Qing Ma, and Jian-Wei Qiu. Multiplicative Renormalizability of Operators defining Quasiparton Distributions. *Phys. Rev. Lett.*, 122(6):062002, 2019. doi: 10.1103/PhysRevLett.122.062002.

[19] Zhouyou Fan, Rui Zhang, and Huey-Wen Lin. Nucleon gluon distribution function from 2 + 1 + 1-flavor lattice QCD. *Int. J. Mod. Phys. A*, 36(13):2150080, 2021. doi: 10.1142/S0217751X21500809.

[20] Zhouyou Fan and Huey-Wen Lin. Gluon parton distribution of the pion from lattice QCD. *Phys. Lett. B*, 823:136778, 2021. doi: 10.1016/j.physletb.2021.136778.

[21] Alejandro Salas-Chavira, Zhouyou Fan, and Huey-Wen Lin. First Glimpse into the Kaon Gluon Parton Distribution Using Lattice QCD. 12 2021.

[22] Tanjib Khan et al. Unpolarized gluon distribution in the nucleon from lattice quantum chromodynamics. *Phys. Rev. D*, 104(9):094516, 2021. doi: 10.1103/PhysRevD.104.094516.

[23] Zhouyou Fan, William Good, and Huey-Wen Lin. Gluon parton distribution of the nucleon from (2 + 1 + 1)-flavor lattice qcd in the physical-continuum limit. *Phys. Rev. D*, 108:014508, Jul 2023. doi: 10.1103/PhysRevD.108.014508.

[24] Robert G. Edwards and Balint Joo. The Chroma software system for lattice QCD. *Nucl. Phys. B Proc. Suppl.*, 140:832, 2005. doi: 10.1016/j.nuclphysbps.2004.11.254.